Electronic Supplementary Material (ESI) for Journal of Materials Chemistry C.

Supporting information for Programmable anisotropic digital metasurface for independent manipulation of dual-polarized THz waves based on voltage-controlled phase transition of VO2 microwires

Javad Shabanpour*

Department of Electrical Engineering, Iran University of Science and Technology, Narmak, Tehran 16486-13114, Iran

E-mail: m.javadshabanpour1372@gmail.com

1. Detailed information of the meta-particle

The meta-particle composed of three metallic layers and two dielectric layers. Figure S1a and S1b represent the metallic patterns on the second and bottom metallic layer as negative and positive electrodes respectively. Two metallic via holes are drilled through the top substrate to connect one of the two electrical contacts for each VO2 microwires (marked with a negative sign in Fig. 1b) and the second metallic layer (ground plane) as a negative electrode. Two metallic via holes are drilled through the top and bottom substrates to attach other electrical contacts (marked with a positive sign in Fig. 1b) with two pieces of separated patches on the bottom metallic layer which act as positive electrodes to apply the DC bias voltage. To ensure that the positive metallic via holes are electrically isolated from the negative electrode (ground plane), we subtracted a metal ring from the second metallic layer. These two via holes are independently connected to two DC bias voltage along x- and y-direction by the means of two separated patches on the bottom metallic layer which are denoted by V_x and V_y respectively in Figure S1b.

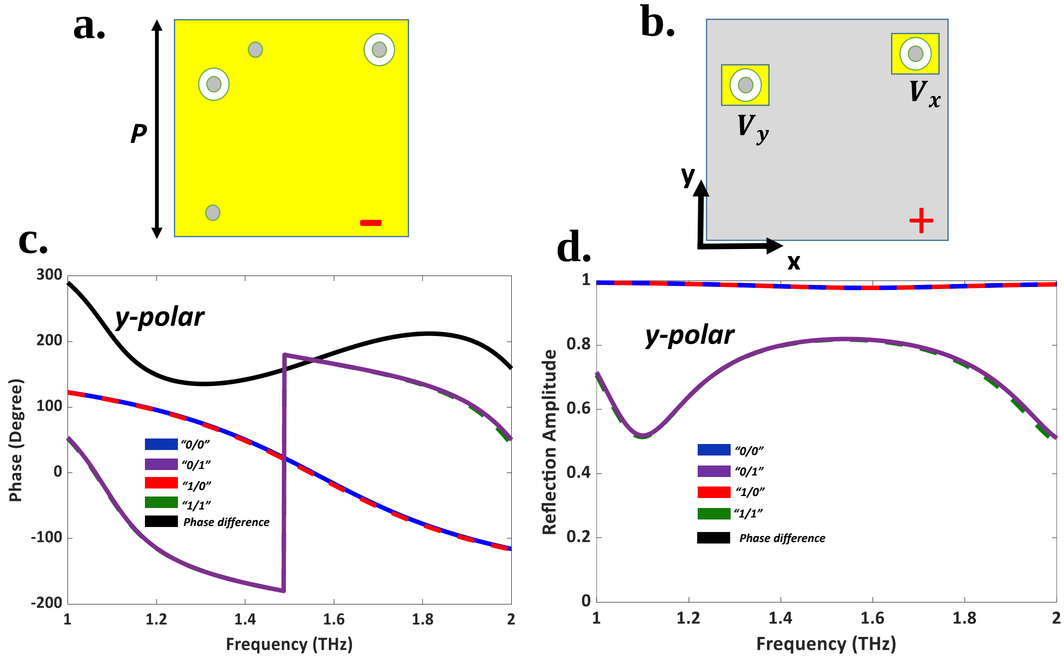

Figure S 1: The two dimensional view a) of the top metallic layer (ground plane) as a negative electrode. b) two pieces of separated patches on the bottom metallic layer which act as positive electrodes to apply the DC bias voltage that are electrically isolated from the negative electrode. Simulated reflection spectra c) phase and d) amplitude of VO2 based meta-particle under illuminating y-polarized excitation.

The conductivity of VO2 microwire along x-direction denoted by δ_x while that along y-direction is denoted by δ_y. The amplitude and phase of reflection for both orthogonal polarizations are depicted in Figure S1(c-d). By switching the electrical conductivity between two states of δ_{off}=$10S/m$ and δ_{on}=$5 \times 10^5 S/m$, four digital states of "0/0," "0/1," "1/0," and "1/1" are obtained.

According to Figure S1(c-d) by changing δ_x, the reflection responses for y-LP incident wave remain fixed. In the same way, the phase and amplitude of reflection for x-LP wave is not influnce by the change of δ_y. This feature exhibits a negligible polarization cross-

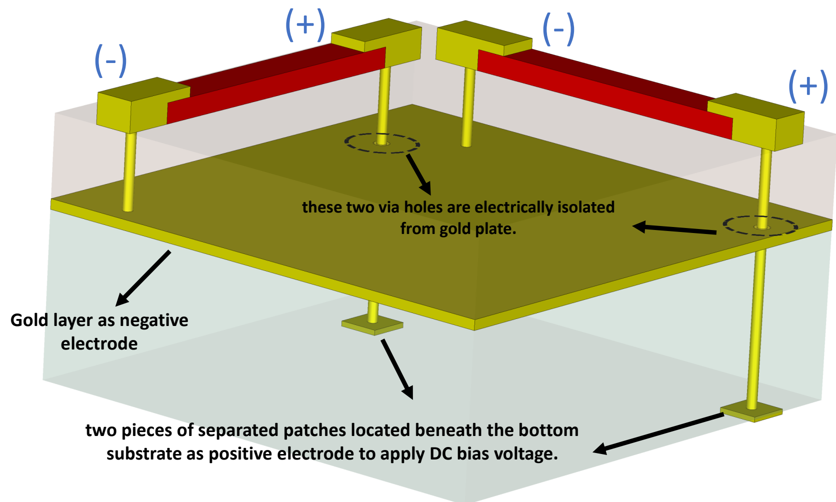

Figure S 2: Schematic of the meta-atom in which the two dielectric layers are hidden. Gold layer act as negative electrode and the two pieces of separated patches act as positive electrodes. The patch along x- and y-direction are independently connected to two DC bias voltage networks.

talk which is of great importance in engineering the THz wavefront independently for two orthogonal polarizations.

Independent reconfigurable reflection responses for two polarizations can also be confirmed by the electric-field distributions of meta-particle. Figure S2 displays the electric-field distributions for four different states of δ_x/δ_y excited by x- and y-LP wave at the operation frequency of 1.5 THz. By switching δ_x from 10 S/m to $5 \times 10^5 S/m$, the electric field distribution for y-LP incident wave remains constant, and similarly, the electric field excited by x-LP wave is not affected by the change of δ_y. Therefore, we can obtain anisotropic digital metasurface with interchangeable missions independently for two orthogonal linearly polarized THz wavefront excitations with negligible polarization cross-talk.

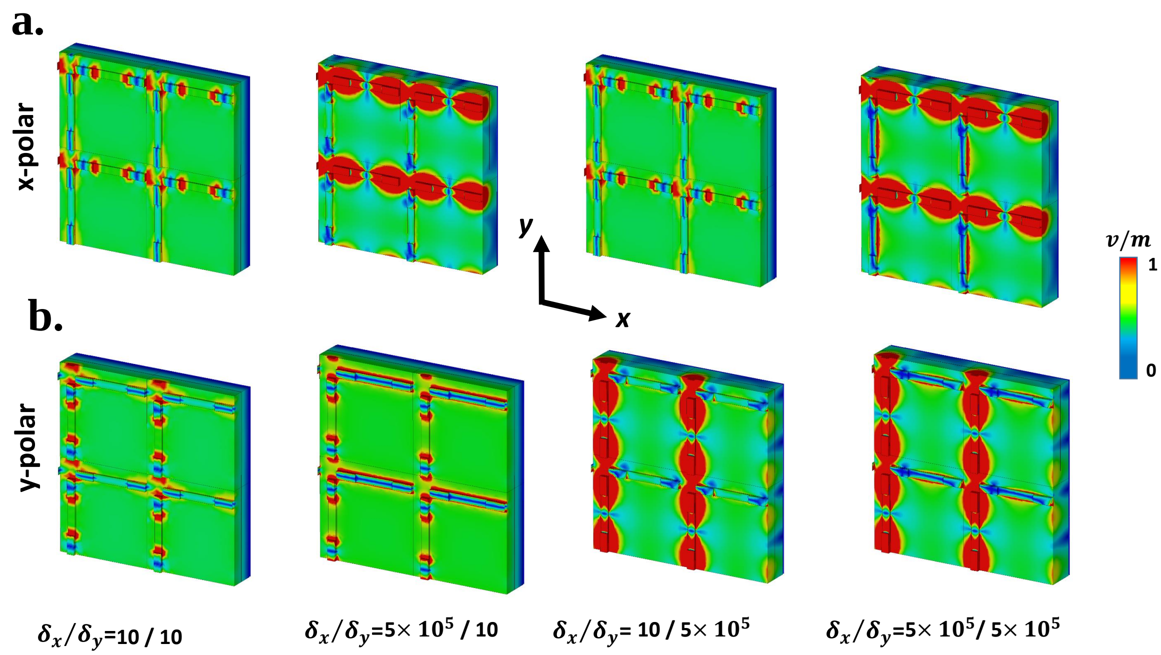

Figure S 3: The surface current distributions of the meta-particle under illumination of a) x-LP b) y-LP. The numbers before and after the slash symbol (/) demonstrates the electrical conductivity of the VO2 microwires along x-direction and y-direction, respectively.

2. Mechanism of MIT in thin VO2 film

It is valuable to mention that the main mechanism of voltage/current driven MIT process in VO2 thin films is still under dynamic investigations and remains controversial. Recently, zimmers et al[1] claim that the local Joule heating plays a predominant role in the dc voltage/current induced MIT in VO2 thin wires. Contrary, the viewpoint of Wu et al[2] was that the Joule heating effect was insignificant and the electric field alone is sufficient to induce MIT. Beyond these two competing claims, some articles were reported that it is difficult to disentangle these two effects in the voltage/current driven MIT process in VO2 thin wires.[3,4] Up to now, VO2 thin films have been prepared on different substrates as silica glass,[5] polyimide,[6] silicon[7] and sapphire[8] by several techniques from chemical vapor deposition[9] to reactive electron-beam evaporation,[10] but it is preferred to use sapphire substrate to reach high-quality VO2 thin films due to the beneficial lattice matching effect. Matching of lattice structures between two different semiconductor materials occurs when two materials with almost equal lattice constants are deposited on top of each other. The lattice constant refers to the physical dimension of unit cells in a crystal lattice. Lattices in three dimensions generally have three lattice constants, referred to as a, b, and c. The lattice mismatch (f) is always the relative difference between the in-plane lattice constants (a) of semiconductor and layer.[11]

$$f = \frac{a_{sub} - a_{layer}}{a_{sub}} \times 100 \tag{1}$$

The lattice mismatch induced defects that are generally degrade the performance of the device. When two dissimilar materials with different lattice parameters are deposited on top of each other, it is reasonable to expect that the interface is highly stressed. Depends on the magnitude of the stress and the thickness of the layers, the interface can be relaxed by forming defects such as dislocations and other unwanted defects. Such defects in general degrade the performance of the devices fabricated.[12] In the case of VO2 grown on silicon substrate, Zhang et al.[13] shown that the defect arising from the lattice mismatch can significantly reduce the resistivity change during the phase transition. On the other hand, depositing VO2 on sapphire substrate[13] exhibiting more than four orders of magnitude resistivity change across the MIT, being among the highest values reported for thin films. Therefore, to achieve the maximum change of resistivity of VO2 film during MIT, sapphire substrate is the best choice.

3. Additional example of VBAM

3.1 Beam steering

To decrease the EM coupling between the adjacent meta-particles, the proposed anisotropic digital metasurface consists of $N \times N$ array of $M \times M$ identical subwavelength meta-particle. The length of the whole structure equals to NMP. The far-field scattering pattern of the structure can be expressed by:[14]

$$E_{sca}(\theta, \varphi) = E_{elem}(\theta, \varphi) \times F(\theta, \varphi) \tag{2}$$

$$F(\theta,\varphi)=\sum_{m=1}^{N}\sum_{n=1}^{N}a_{mn}\exp\left[-j\left\{\varphi(m,n)+KP\sin\theta\left[(m-1/2)\cos\varphi+(n-1/2)\sin\varphi\right]\right\}\right] \tag{3}$$

where θ, φ, P, a_{mn}, φ_{mn} represent the elevation and azimuth angles of the scattered beams, period of lattices and reflection amplitude and phase of each lattice respectively.

To show the beam steering properties of the proposed structure, we encode the metasurface with coding sequence of (0101.../0101...) with different lattice sizes. According to generalized Snell's law, the deviation angles can be calculated as $\sin^{-1}(\lambda/2MP)$. Obviously, by changing the dimension of the lattices one can adjust the deviation angle in a real-time manner independent for dual-polarized incidents. Figure S3 demonstrates the 3D far-field scattering patterns for different values of M which is define as the number of meta-particles in one lattice. Good agreement between full wave simulations and theoretical predictions verify the validity of the presented beam steering analysis in the proposed anisotropic VO2-assisted digital metasurface.

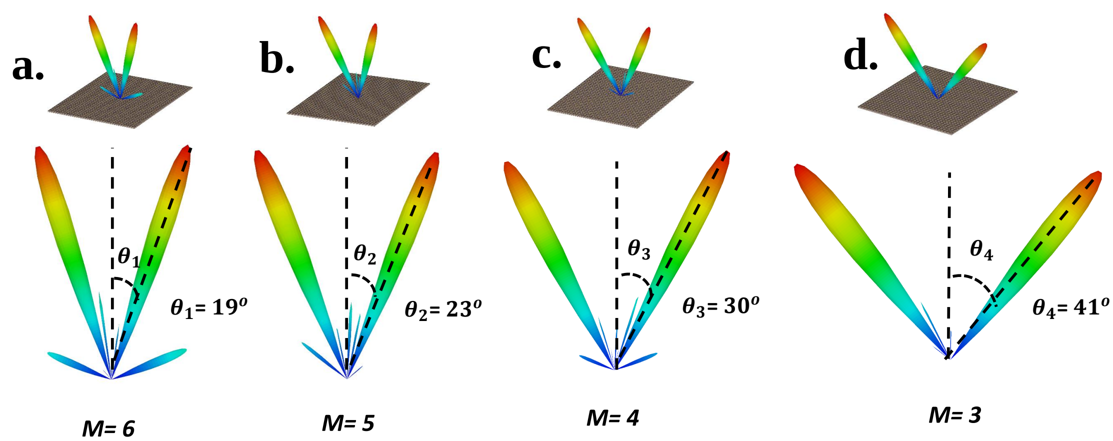

	M=6	M=5	M=4	M=3
$\theta = \sin^{-1}\left(\frac{\lambda}{2MP}\right) = \sin^{-1}\left(\frac{2}{M}\right)$	θ_1= 19.47^o	θ_2= 23.5^o	θ_3= 30^o	θ_4= 41.8^o

Figure S 4: Schematic of 1-bit VBAM driven by coding sequence of (0101.../0101...) and its 3D far-field scattering patterns for a) M=6, b) M=5, c) M=4, d) M=3. Comparison between full wave simulations and theoretical predictions also provided in the table.

3.2 Focused vortex beam

The versatility of the proposed anisotropic metasurface also has armed a platform to obtain focused vortex beams with ultrafast switching time between different OAM modes and focal lengths. Toward this aim, the spatial phase profile on the metasurface must include both spiral and parabolic phase distributions simultaneously which can be expressed by:[15]

$$\varphi(x, y) = l \times \tan^{-1}(\frac{y}{x}) + \frac{2\pi}{\lambda}\left(\sqrt{x^2 + y^2 + z_f^2} - z_f\right) \tag{4}$$

For y-LP incident THz waves, we encode the VBAM with spiral-parabola phase distributions in such a way to generate focused vortex wavefront with OAM modes l=-1 1in focal spot of x=0, y=0, z=200μm. At the same time, by driving the VBAM with suitable phase profile under x-LP excitations, focused vortex wavefront with OAM modes l=-2 in focal spot of x=400μm, y=-200μm, z=200μm was satisfactorily generated. Furthermore, the focal point and topological charges of the corresponding focused vortex beams can be dynamically tuned by mere changing the biasing voltage. 2D near-field patterns of such encoded VBAM as well as the spatial phase profile on the metasurface, are depicted in Figure S4.

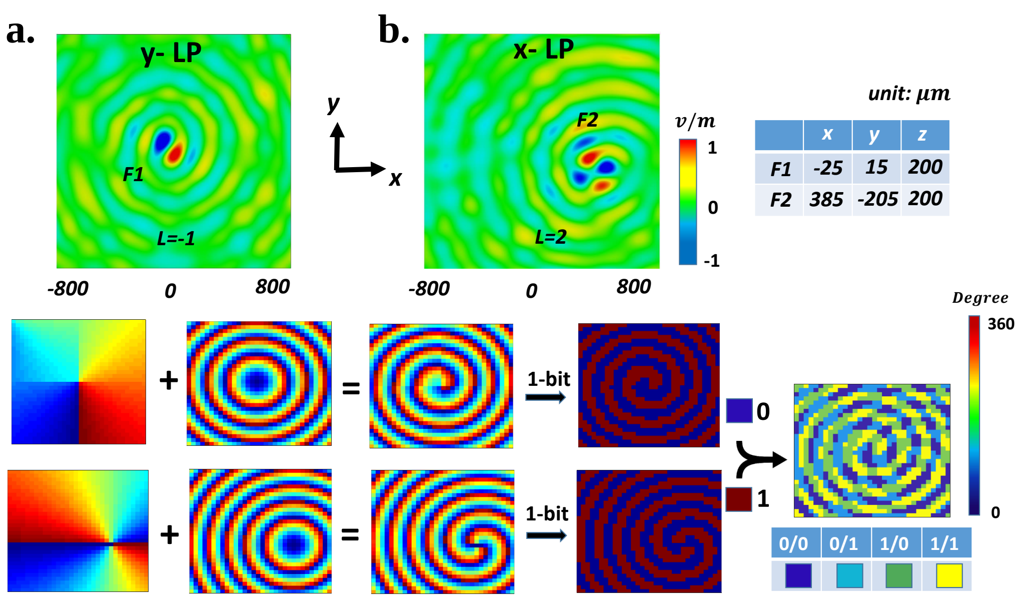

Figure S 5: 2D near-field patterns of VBAM encoded with spiral-parabola phase distribution a) Focused vortex wavefronts with OAM mode l=-1 located at x=-25μm, y =-15μm , z = 200μm. b) Focused vortex wavefronts with OAM mode l=-2 located at x=385μm, y=-205μm, z=200 μm. c) Required phase distribution for generating the aforementioned focused vortex wavefronts.

References

(1) Zimmers, A.; Aigouy, L.; Mortier, M.; Sharoni, A.; Wang, S.; West, K.; Ramirez, J.; Schuller, I. K. Role of thermal heating on the voltage induced insulator-metal transition in VO 2. *Physical review letters* **2013**, *110*, 056601.

(2) Wu, B.; Zimmers, A.; Aubin, H.; Ghosh, R.; Liu, Y.; Lopez, R. Electric-field-driven phase transition in vanadium dioxide. *Physical Review B* **2011**, *84*, 241410.

(3) Joushaghani, A.; Jeong, J.; Paradis, S.; Alain, D.; Stewart Aitchison, J.; Poon, J. K. Voltage-controlled switching and thermal effects in VO2 nano-gap junctions. *Applied Physics Letters* **2014**, *104*, 221904.

(4) Liao, G.; Chen, S.; Fan, L.; Chen, Y.; Wang, X.; Ren, H.; Zhang, Z.; Zou, C. Dynamically tracking the joule heating effect on the voltage induced metal-insulator transition in VO2 crystal film. *AIP Advances* **2016**, *6*, 045014.

(5) Wen, Q.-Y.; Zhang, H.-W.; Yang, Q.-H.; Xie, Y.-S.; Chen, K.; Liu, Y.-L. Terahertz metamaterials with VO 2 cut-wires for thermal tunability. *Applied physics letters* **2010**, *97*, 021111.

(6) Lv, T.; Li, Y.; Ma, H.; Zhu, Z.; Li, Z.; Guan, C.; Shi, J.; Zhang, H.; Cui, T. Hybrid metamaterial switching for manipulating chirality based on VO 2 phase transition. *Scientific reports* **2016**, *6*, 23186.

(7) Xiao, D.; Kim, K.; Zavada, J. Electrically programmable photonic crystal slab based on the metal-insulator transition in VO 2. 2005.

(8) Kim, Y.; Wu, P. C.; Sokhoyan, R.; Mauser, K.; Glaudell, R.; Kafaie Shirmanesh, G.; Atwater, H. A. Phase modulation with electrically tunable vanadium dioxide phase-change metasurfaces. *Nano letters* **2019**, *19*, 3961–3968.

(9) Sahana, M.; Subbanna, G.; Shivashankar, S. Phase transformation and semiconductor-metal transition in thin films of VO 2 deposited by low-pressure metalorganic chemical vapor deposition. *Journal of applied physics* **2002**, *92*, 6495–6504.

(10) Lee, M.-H.; Kim, M.-G. RTA and stoichiometry effect on the thermochromism of VO2 thin films. *Thin solid films* **1996**, *286*, 219–222.

(11) Melton, W. A.; Pankove, J. I. GaN growth on sapphire. *Journal of crystal growth* **1997**, *178*, 168–173.

(12) Qing-Xuan, Y.; Bo, X.; Qi-Hong, W.; Yuan, L.; Guan-Zhong, W.; Rong-Chuan, F. Growth of ZnO thin films on lattice-matched substrates by pulsed-laser deposition. *Chinese physics letters* **2003**, *20*, 2235.

(13) Zhang, H.-T.; Zhang, L.; Mukherjee, D.; Zheng, Y.-X.; Haislmaier, R. C.; Alem, N.; Engel-Herbert, R. Wafer-scale growth of VO 2 thin films using a combinatorial approach. *Nature communications* **2015**, *6*, 8475.

(14) Cui, T. J.; Qi, M. Q.; Wan, X.; Zhao, J.; Cheng, Q. Coding metamaterials, digital metamaterials and programmable metamaterials. *Light: Science & Applications* **2014**, *3*, e218–e218.

(15) Ma, X.; Pu, M.; Li, X.; Huang, C.; Wang, Y.; Pan, W.; Zhao, B.; Cui, J.; Wang, C.; Zhao, Z., et al. A planar chiral meta-surface for optical vortex generation and focusing. *Scientific reports* **2015**, *5*, 10365.